Capillarity

Vol. 19, No. 3, p. 75-85, 2026

Original article

Reconstructing the hydraulic conductivity model of freezing soils based on lubrication theory

Ceting Yu[1,2], Fugang Wang[1,2]*, Cheng Hui[1,2], Longxuan Li[1,2], Shilin Zhang[3], Shengwei Li[4]*

[1]*Key Laboratory of Groundwater Resources and Environment, Ministry of Education, Jilin University, Changchun 130012, P. R. China*
[2]*Jilin Province Key Laboratory of Water Resources and Water Environment, Changchun 130012, P. R. China*
[3]*Yanbian Branch of Jilin Provincial Bureau of Hydrology and Water Resources, Yanbian 133613, P. R. China*
[4]*Chengdu Center, China Geological Survey, Chengdu 610081, P. R. China*

Keywords:
Frozen soil
hydraulic conductivity
lubrication theory
film flow

Cited as:
Yu, C., Wang, F., Hui, C., Li, L., Zhang, S., Li, S. Reconstructing the hydraulic conductivity model of freezing soils based on lubrication theory. Capillarity, 2026, 19(3): 75-85.
https://doi.org/10.46690/capi.2026.06.02

Abstract:
Accurate characterization of hydraulic conductivity is essential for understanding coupled heat and water transport during soil freezing and thawing. However, conventional models can produce a nonphysical conductivity cutoff under strong supercooling because they oversimplify film driven transport. Here, an existing combined capillary-film framework is extended by deriving a physically based expression for film flow conductivity. Using established film-thickness relationships to define the geometry, classical lubrication theory is applied to quantify flow velocity and hydraulic conductivity within thin adsorbed water films. Integrating this lubrication based expression with the capillary flow equation yields a continuous hydraulic conductivity model without an artificial dry-end cutoff. Validation against diverse unfrozen and frozen soil datasets shows that the model performs consistently across the full moisture range and avoids the dry-end failure of the Campbell and van Genuchten models. Parameter sensitivity analyses further clarify how film flow responds to particle radius and porosity. Smaller particles provide greater specific surface area to sustain film flow at low water contents, whereas lower porosity delays the transition from capillary dominated to film dominated transport. The model therefore provides a physically interpretable basis for representing continuous unfrozen-water migration in frozen soils.

1. Introduction

Unfrozen water migration during freezing and thawing is a key process governing coupled heat and water transport and associated geotechnical hazards, including frost heave, in cold regions (Taber, 1930; Chen et al., 2023). The magnitude and rate of this redistribution are strongly controlled by the hydraulic conductivity of frozen soil (Watanabe and Flury, 2008). As subzero temperatures decrease, the progressive formation of pore ice severely occludes macroscopic capillary channels, forcing liquid water to migrate through highly restricted, microscopic pathways (Tokunaga, 2009; Lebeau and Konrad, 2010; Ming et al., 2022). Accurately characterizing the evolution of hydraulic conductivity under subzero conditions remains challenging (Ireson et al., 2013; Painter et al., 2013; Walvoord and Kurylyk, 2016). A physically based model of unfrozen water conductivity is therefore needed to improve cryohydrological simulations and assessments of engineering risk in permafrost environments (Kurylyk et al., 2014; Lamontagne-Hallé et al., 2020).

Yandy Scientific Press

*Corresponding author.
E-mail address: yuct21@mails.jlu.edu.cn (C. Yu); wangfugang@jlu.edu.cn (F. Wang); chenghui22@mails.jlu.edu.cn (C. Hui); lilx25@mails.jlu.edu.cn (L. Li); shilin2867@sohu.com (S. Zhang); 13808073872@163.com (S. Li).

Received April 21, 2026; revised May 20, 2026; accepted June 9, 2026; available online June 11, 2026.

Moisture migration in frozen soils is commonly described using Darcy's law, which requires an accurate hydraulic conductivity function. Historically, various empirical and semi-empirical models have been proposed to characterize this parameter as a function of temperature or unfrozen water content (Campbell, 1974; van Genuchten, 1980; Jin et al., 2019). However, many empirical models become numerically unstable or predict an abrupt cutoff to zero conductivity when soil is strongly supercooled and capillary pathways are occluded by ice (Zhang et al., 2021; Li et al., 2024). While alternative approaches integrating the soil freezing characteristic curve with particle gradation provide a more structured framework (Azmatch et al., 2012; Wang and Vanapalli, 2025), their fitted parameters often lack clear physical interpretations of pore scale water transport.

Although the conceptual distinction between capillary and film water is now widely recognized in soil physics (Tokunaga, 2009; Ming et al., 2022), a critical deficiency in current dual-mechanism frameworks is the lack of a rigorous, physically derived mathematical model for the film flow component itself. When macroscopic capillary flow becomes negligible, existing models predominantly rely on highly simplified or purely empirical functions to represent film conductivity (Tang et al., 2019; Ming et al., 2022). These models do not explicitly resolve the viscous hydrodynamics of thin adsorbed layers described by lubrication theory. This missing hydrodynamic basis can cause systematic underestimation and nonphysical cutoffs of hydraulic conductivity in deeply frozen soils.

Considerable progress has been made in elucidating the thermodynamic mechanisms governing unfrozen water content and equilibrium film thickness (Dash et al., 2006; Hansen-Goos and Wettlaufer, 2010). However, translating these equilibrium geometric properties into dynamic flow parameters remains difficult. Current macroscopic models often bypass the fluid mechanics of these liquid-like layers and use empirical approximations that do not explicitly represent viscous resistance near particle surfaces (Golparvar et al., 2018; Zhao et al., 2023; Zhou et al., 2023). Bridging this gap requires moving beyond thermodynamics to explicitly integrate classical lubrication theory, which can rigorously quantify the velocity profile and shear stress within these tightly adsorbed films (Wan and Tokunaga, 1997). Resolving this hydrodynamic link is important under strong supercooling, when capillary pathways become disconnected and film flow becomes increasingly important (Saruya et al., 2014; Lan et al., 2025).

Rather than redefining the capillary-film framework, this study derives its film flow conductivity term from lubrication theory and Newton's law of viscosity. Using established film thickness relationships as the geometric basis, lubrication theory is applied to quantify velocity profiles and the resulting film permeability. The combined model is evaluated against diverse soil datasets and compared with classical empirical models. The effects of particle radius and porosity on the partitioning between capillary and film transport are also examined.

2. Mathematical model construction

Representing water transport across the full moisture range in frozen soils requires distinct descriptions of liquid flow at different scales. Macroscopic flow is primarily governed by capillary forces within the pore space, whereas at higher degrees of supercooling, water migration is restricted to thin, adsorbed films covering soil particles. This transition resembles the hydraulic behavior of very dry unfrozen soils. In both cases, the connected capillary water phase becomes limited, either because water content decreases during drying or because pore ice occupies part of the pore space during freezing. The remaining liquid water is then mainly retained as adsorbed films on particle surfaces, so film flow becomes increasingly important for maintaining a nonzero hydraulic conductivity. In this study, a combined capillary-film scheme is adopted to integrate these two flow regimes into a unified mathematical framework. The following sections describe the selection of the capillary model and the hydrodynamic derivation of the film flow component, which together form the basis for a continuous hydraulic conductivity function.

When the unfrozen water content is relatively high, moisture migration is predominantly governed by capillary forces within the macroscopic pore network. In this wet regime, hydraulic conductivity decreases nonlinearly as liquid saturation declines. Following the classical pore size distribution model of Campbell (1974), capillary hydraulic conductivity is expressed as (Wang et al., 2016):

$$K_c = K_s S_c^l \left[1 - \left(\frac{1 - S^{1/m}}{1 - S_r^{1/m}} \right)^{1-1/n} \right]^2 \tag{1}$$

The unsaturated hydraulic conductivity, K_c, is defined as a function of the saturated hydraulic conductivity, K_s, and the effective saturation, S_c, as expressed in the following equation. In this equation, l represents the pore-connectivity parameter, while m and n denote empirical shape parameters related to the pore-size distribution, typically constrained by $m = 1 - 1/n$. The terms S and S_r correspond to the degree of saturation and the residual saturation, respectively. Here, the degree of saturation S is defined as the ratio of the unfrozen water content θ to the saturated volumetric water content θ_s. It should be noted that in a fully saturated soil matrix prior to freezing, θ_s is physically equivalent to the initial soil porosity ϕ.

Calculating film flow conductivity first requires a relationship between film water thickness and capillary potential. In partially saturated porous media, film thickness can be estimated by normalizing volumetric water content by specific surface area. This approximation is most applicable at low water contents, where adsorption is the dominant retention mechanism.

Wan and Tokunaga (1997) estimated the hydraulic properties of unsaturated porous media by considering how surface tension and particle diameter affect surface water films. The expression is as follows:

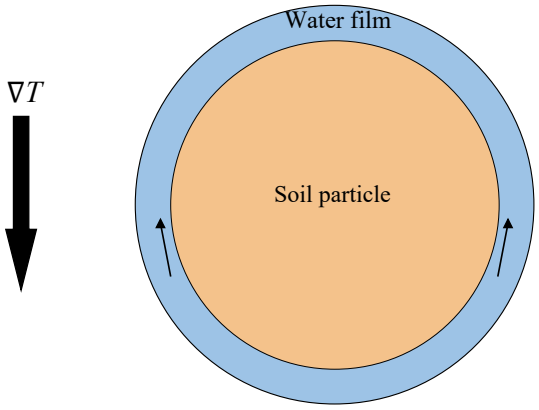

Fig. 1. Schematic of water film flow around a soil particle under a temperature gradient.

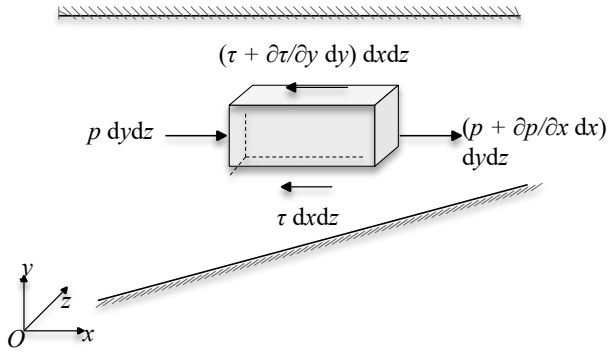

Fig. 2. Force balance of an infinitesimal element in water film flow.

$$\chi = \sqrt{\frac{\varepsilon\varepsilon_0}{2}}\left(\frac{\pi k_B T_m}{ze}\right)\left[\frac{4\sigma_{sl}}{R} - f(S)\right]^{-1/2} \tag{2}$$

The equation for the film dynamics under electrostatic influence is derived from the theoretical framework of Rempel et al. (2004) and its application to freezing porous media (Wettlaufer, 1999). The parameter χ is determined based on the electrochemical and interfacial properties of the system, where ε and ε_0 represent the relative permittivity and the vacuum permittivity, respectively. The term k_B denotes the Boltzmann constant, T_m is the absolute melting temperature, z is the ion valence, and e represents the elementary charge. Additionally, σ_{sl} signifies the solid-liquid interfacial tension, R is the characteristic pore radius, and $f(S)$ is a function of the degree of saturation.

Film flow is treated as one-dimensional and vertical, and the film thickness at the warm end is denoted by f. Under a supercooling of ΔT, the film water migrates toward the cold end. The physical configuration of water film flow around a soil particle is shown in Fig. 1. By establishing a conservation equation using a simplified micro-unit model, a velocity equation can be derived for solving the flow dynamics.

The force balance of an infinitesimal element in the water film is shown in Fig. 2. The pressure exerted on the liquid surface of this element is then analyzed along the x-coordinate.

Along the x-coordinate, the pressures on the left and right faces are $p+(\partial p/\partial x)\mathrm{d}x$ and p. The shear stresses on the upper and lower surfaces are given by τ and $\tau+(\partial\tau/\partial y)\mathrm{d}y$.

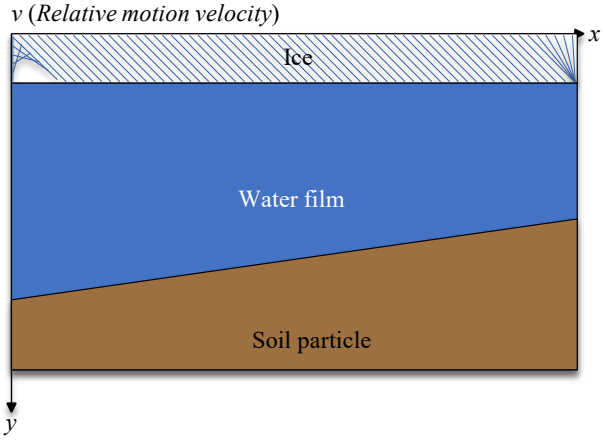

Fig. 3. Lubrication theory schematic for relative motion between two parallel plates.

The force balance along the x-coordinate is:

$$p\mathrm{d}y\mathrm{d}z + \tau\mathrm{d}x\mathrm{d}z = \left(p + \frac{\partial p}{\partial x}\mathrm{d}x\right)\mathrm{d}y\mathrm{d}z + \left(\tau + \frac{\partial\tau}{\partial y}\mathrm{d}y\right)\mathrm{d}x\mathrm{d}z \tag{3}$$

Applying the Navier-Stokes equations to this thin film geometry gives:

$$\frac{\partial p}{\partial x} = \frac{\partial\tau}{\partial y} \tag{4}$$

The above equations indicate that the pressure gradient in the x direction is balanced by the gradient of shear stress in the y direction within the water film. For a Newtonian fluid, shear stress is:

$$\tau = -\mu\frac{\partial u}{\partial y} \tag{5}$$

Substituting the constitutive relationship of shear stress into the momentum balance yields the governing equation for the local velocity field:

$$\frac{\partial\tau}{\partial y} = -\mu\frac{\partial^2 u}{\partial y^2} \tag{6}$$

Integrating Eq. (6) once with respect to y gives the shear rate distribution:

$$\frac{\partial u}{\partial y} = \frac{1}{\mu}\frac{\partial p}{\partial x}y + C_1 \tag{7}$$

A second integration gives the velocity profile in the water film:

$$u(y) = \frac{1}{2\mu}\frac{\partial p}{\partial x}y^2 + C_1 y + C_2 \tag{8}$$

where C_1 and C_2 are integration constants. For a water film with thickness f, the lower boundary is fixed and the upper boundary moves with a relative velocity v. Under the no slip condition, the boundary conditions are: $u(0)=0$, $u(f)=v$. The simplified lubrication geometry used to determine the boundary conditions is shown in Fig. 3.

Substituting these boundary conditions into Eq. (8), the velocity distribution in the water film can be obtained as:

$$u(y) = \frac{v}{f}y + \frac{1}{2\mu}\frac{\partial p}{\partial x}\left(y^2 - fy\right) \tag{9}$$

The average velocity of film water is then obtained by integrating the velocity distribution across the film thickness:

$$\bar{u} = \frac{1}{f}\int_0^f u(y)\mathrm{d}y = \frac{v}{2} - \frac{f^2}{12\mu}\frac{\partial p}{\partial x} \tag{10}$$

In Eq. (10), the first term represents the contribution induced by the relative motion of the upper boundary, whereas the second term represents the pressure driven flow within the water film. For the basic frozen soil formulation, pore ice and soil particles are treated as a relatively stationary solid framework. Under this condition, the macroscopic relative velocity at the ice water interface is taken as $v = 0$, and the Couette flow contribution in Eq. (10) vanishes.

This assumption is most applicable when the liquid film is mainly driven by the pressure gradient and the ice particle framework remains stable. If interfacial slip or relative motion occurs, the first term in Eq. (10) should be retained or modified by introducing a slip velocity or slip length. Such a correction may change the magnitude of the film hydraulic conductivity, especially when the interfacial velocity is comparable to the pressure driven film velocity, but it does not change the pressure driven lubrication term derived here. Therefore, the $v = 0$ formulation is used as a baseline case for frozen soils with a relatively stable ice particle framework. Under this assumption, Eq. (10) reduces to:

$$\bar{u} = -\frac{f^2}{12\mu}\frac{\partial p}{\partial x} \tag{11}$$

Multiplying the average film velocity by the effective cross sectional area occupied by film water gives the film flow rate:

$$Q_f = -(1 - S_c)A_f\frac{f^3}{12\mu}\frac{\partial p}{\partial x} \tag{12}$$

where Q_f is the film flow rate, S_c is the capillary saturation contribution, and A_f is the effective cross sectional area factor of film water. Here, A_f represents the fraction of the nominal pore cross section that can actually contribute to connected film flow. It accounts for the reduction in flow area caused by incomplete film coverage, disconnected adsorbed water, and the tortuous geometry of film pathways. Therefore, the effects commonly described by film connectivity and tortuosity factors are included in A_f in an effective form rather than introduced as separate empirical parameters.

Physically, A_f is dimensionless and should be constrained within ($0 < A_f \leq 1$). A value close to 1 indicates that the adsorbed film remains relatively continuous along the solid surface, whereas a smaller value represents stronger film disconnection or a more restricted flow path. In the absence of direct pore scale measurements, A_f can be determined by fitting the low water content portion of the hydraulic conductivity curve, where film flow becomes the dominant transport mechanism. During fitting, A_f was constrained within its physical range to avoid an unconstrained empirical adjustment:

$$K_f = (1 - S_c)A_f\frac{f^3}{12\mu} \tag{13}$$

According to Eq. (13), A_f affects K_f linearly. Therefore, increasing or decreasing A_f changes the magnitude of the film flow contribution in the same proportion, while it does not change the cubic dependence of K_f on film thickness f or the pressure driven lubrication mechanism. In this sense, the sensitivity of K_f to A_f is straightforward and mainly controls the amplitude of film conductivity rather than the form of the derived film flow relation.

The total hydraulic conductivity is then obtained by adding the capillary flow contribution and the film flow contribution:

$$K_t(\theta) = K_c(\theta) + K_f(\theta) \tag{14}$$

where K_t denotes the total hydraulic conductivity, and the subscript t represents total. In this formulation, f is used consistently to denote the local water film thickness. The subscript f is used only for quantities associated with film flow, such as Q_f and K_f, and is not used as a thickness variable. Therefore, the final expression links the film flow contribution directly to water film thickness, water viscosity, effective flow area, and the pressure gradient.

In the combined capillary-film formulation, θ_r is used to describe the water content level at which the dominant transport mechanism changes from capillary flow to film flow. It is not introduced as an artificial cutoff value. Instead, it marks the transition range where the capillary contribution rapidly decreases and the film flow contribution becomes increasingly important. In this study, θ_r is determined from the water retention parameters used in the capillary conductivity function and is further checked by comparing the relative magnitudes of K_c and K_f. When K_f becomes comparable to or greater than K_c, the model enters the film dominated regime. Therefore, θ_r should be understood as a physically based transition indicator rather than a numerical switch.

3. Model validation and discussion

Model performance was assessed using soil hydraulic datasets that extend to very low water contents. Sixteen datasets spanning sand, loamy sand, sandy loam, loam, sandy clay, and clay were selected. Soils 1-12 corresponded to those used by Lebeau and Konrad (2010) and were documented in several earlier studies (Pachepsky et al., 1984; Mehta et al., 1994; Nemes et al., 2001; Fujimaki and Inoue, 2003). Additionally, four clay-rich soil samples were extracted from the UNSODA database (Becher, 1971) to assess the model behavior under fine-textured soil scenarios. The validation results for the 16 soil datasets are shown in Fig. 4. Validation parameters were obtained from Wang et al. (2016).

Across the 16 soils, the model captured texture dependent hydraulic behavior, including the sustained conductivity tail in fine grained soils. Root mean square error (RMSE) and the coefficient of determination (R^2) were used to evaluate all validation datasets. Their definitions are given in Eqs. (15) and (16), and the statistical results are summarized in Table 1.

$$\mathrm{RMSE} = \sqrt{\frac{1}{n}\sum_{i=1}^{n}(y_i - \hat{y}_i)^2} \tag{15}$$

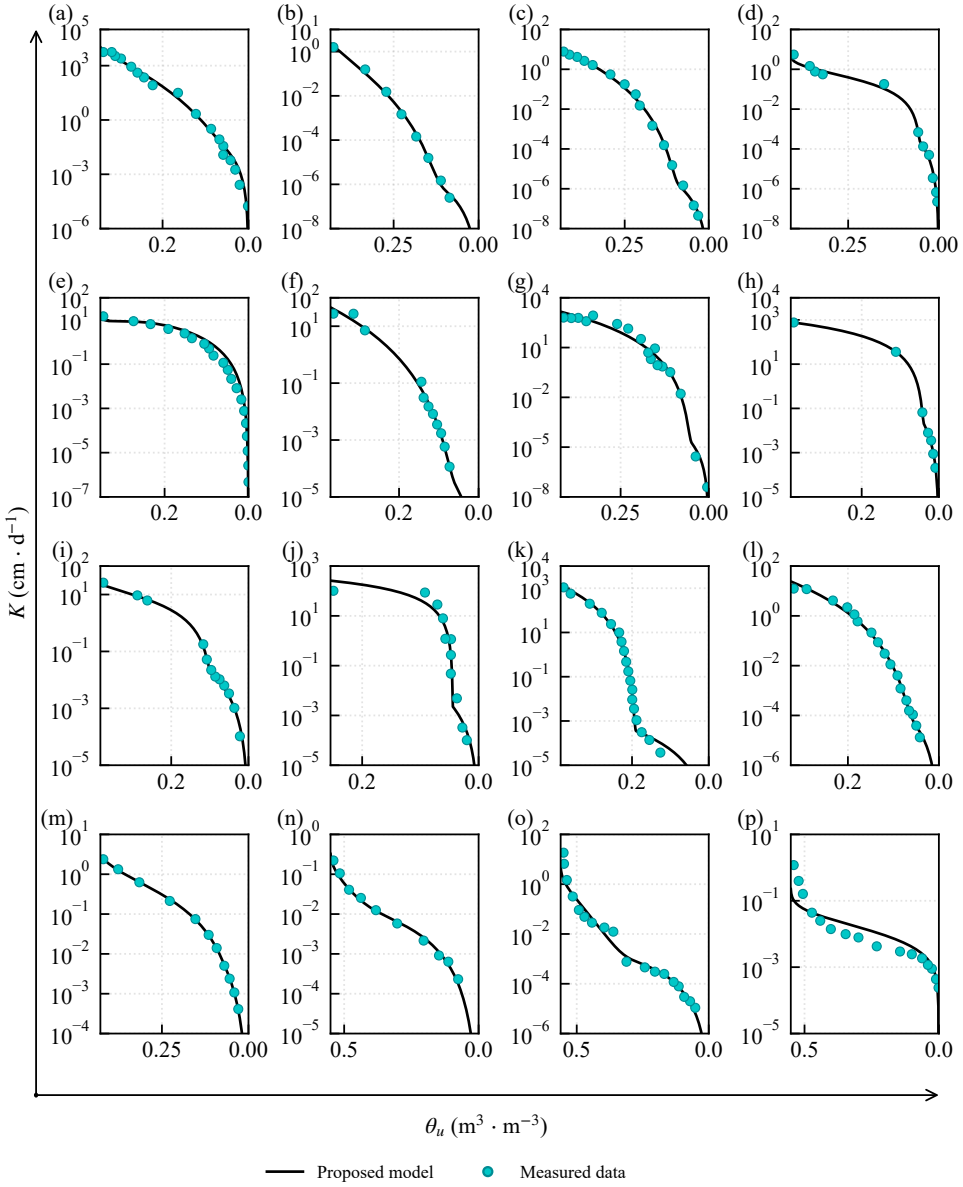

Fig. 4. Model validation of the proposed hydraulic conductivity model against measured data for 16 soils. (a) Masa loamy sand, (b) Adelanto loam, (c) Pachapa loam, (d) Sandy loam, (e) Gilat loam, (f) Poederlee loamy sand, (g) Shonai sand, (h) Berlin medium sand, (i) Poederlee sand, (j) Hupsel sand, (k) Rehevot sand, (l) Pachapa fine sandy clay, (m) Seelow clay 1, (n) Seelow clay 2, (o) Hollern clay 1 and (p) Hollern clay 2.

$$R^2 = 1 - \frac{\sum_{i=1}^{n} (y_i - \hat{y}_i)^2}{\sum_{i=1}^{n} (y_i - \bar{y}_i)^2} \tag{16}$$

where y_i is the measured hydraulic conductivity; $\hat{y}_i$ is the predicted hydraulic conductivity; $\bar{y}_i$ is the mean value of the measured hydraulic conductivity; and n is the number of data points.

To further examine the applicability of the proposed model to freezing soils, an additional validation was performed using the frozen soil hydraulic conductivity data reported by Ming et al. (2020). The dataset includes five frozen soils and covers a wide range of hydraulic conductivity, from approximately 10^{-12} to 10^{-6} cm/s. In this validation, unfrozen water content was used as the state variable, and the proposed capillary and film flow model was fitted to the measured hydraulic conductivity data without imposing an artificial cutoff at low unfrozen water content.

Fig. 5 shows that the proposed model reproduces the measured hydraulic conductivity of five frozen soils across several orders of magnitude. This agreement supports the applicability of the model to frozen soil conditions. Together with the validation against 16 unfrozen soil datasets, where R^2 ranges from 0.76 to 0.88, this frozen soil validation shows that the proposed film flow formulation improves the continuity of hydraulic conductivity prediction over both low water content and freezing conditions. However, this validation should be interpreted within the range of unfrozen water content and

Table 1. Statistical performance of the proposed model.

Soil type	RMSE	R^2
Masa loamy sand	0.3182	0.82
Adelanto loam	0.3740	0.84
Pachapa loam	0.3377	0.82
Sandy loam	0.2340	0.85
Gilat loam	0.1522	0.88
Poederlee loamy sand	0.2060	0.86
Shonai sand	0.7731	0.76
Berlin medium sand	0.2417	0.84
Poederlee sand	0.1794	0.86
Hupsel sand	0.5511	0.78
Rehevot sand	0.4387	0.79
Pachapa fine sandy clay	0.2119	0.88
Seelow clay 1	0.2169	0.86
Seelow clay 2	0.2066	0.86
Hollern clay 1	0.3154	0.82
Hollern clay 2	0.2477	0.87

Table 2. Parameters used in the VG and Campbell models.

Parameter	Gilat loam	Hollern clay 2
α	0.023	0.3740
m	0.2668	0.1868
b	1.58	0.84

hydraulic conductivity covered by the Ming et al. (2020) dataset, and further tests are still needed for soils with extremely high ice content, strong cryosuction gradients, or discontinuous film water pathways.

One sandy soil and one clayey soil were selected to compare the proposed model with the Campbell and van Genuchten (VG) models. Parameters for the VG and Campbell models were calibrated within the ranges reported by Chen et al. (2021) and are summarized in Table 2.

The comparison among the proposed model, the Campbell model, and the VG model is shown in Fig. 6. For the sandy soil, the VG and proposed models agreed with the measurements across the full water content range, whereas the Campbell model showed larger deviations. For the clayey soil, both classical models underestimated hydraulic conductivity at low water contents because they did not fully represent film flow.

The simple power-law Campbell model showed limited agreement for both sandy and clayey soils. The VG model performed better for sandy soil but underestimated hydraulic conductivity in the film-dominated range of the clayey soil. In contrast, the proposed model shows better agreement with the measured data in both soil types.

It should be noted that the present formulation differs from the Lebeau and Konrad type capillary-film framework mainly in the treatment of the film flow term. The capillary-film partitioning concept is retained, but the film conductivity is not prescribed only through a macroscopic empirical correction. Instead, the film flow contribution is derived from the lubrication based velocity profile and is explicitly related to film thickness, water viscosity, effective flow area, and pressure gradient. Therefore, the comparison is not intended to replace the capillary film concept, but to show that the derived film flow term gives a clearer hydrodynamic basis for the low water content conductivity tail.

Four representative soils were selected to illustrate flow partitioning within the combined capillary-film model: Hupsel sand, Masa loamy sand, Gilat loam, and Hollern clay 2. Here, the film flow contribution ratio η is defined as the percentage of total hydraulic conductivity contributed by the film flow component: $\eta = \left[K_f/(K_c + K_f)\right] \times 100\%$. A value of $\eta \to 0$ indicates capillary-dominated transport, while $\eta \to 100\%$ corresponds to pure film flow. As illustrated in the contribution profiles, the transition between capillary and film flow varies with soil texture, specifically the pore-size distribution and the calculated residual water content. In coarse- and medium-grained soils (e.g., Hupsel sand, Masa loamy sand, and Gilat loam), the change in dominant mechanism occurs gradually. The red dashed lines in Fig. 7 represent the theoretically calculated residual water content (θ_r) values for each soil, which mark the onset of film-flow dominance.

The transition range is not identical for all soils because θ_r is controlled by the pore size distribution and the amount of water retained as adsorbed films. In coarse and medium textured soils, such as Hupsel sand, Masa loamy sand, and Gilat loam, the capillary network loses connectivity gradually, so capillary flow and film flow coexist over a relatively broad water content interval before film flow becomes dominant. In contrast, the fine textured Hollern clay 2 shows a sharper transition near the calculated θ_r, reflecting its larger specific surface area and more concentrated micropore structure. This soil dependent transition allows the model to avoid a fixed dry-end cutoff and permits the dominant transport mechanism to shift according to soil texture.

4. Sensitivity analysis of soil structural parameters

The validation results support the performance of the continuous capillary-film model. However, the actual physical process is controlled by the microscopic structure of the soil. To better understand water migration in freezing soils, this section presents a parameter sensitivity analysis focusing on two key variables: The equivalent particle radius (r) and the initial soil porosity (ϕ). In the proposed model, these parameters determine the specific surface area and the total pore space, respectively. By varying these parameters, this analysis aims to quantitatively evaluate how different soil textures and the continuous growth of pore ice (which effectively reduces porosity) influence the shift between capillary flow and film flow. The analysis examines the physical consistency of the

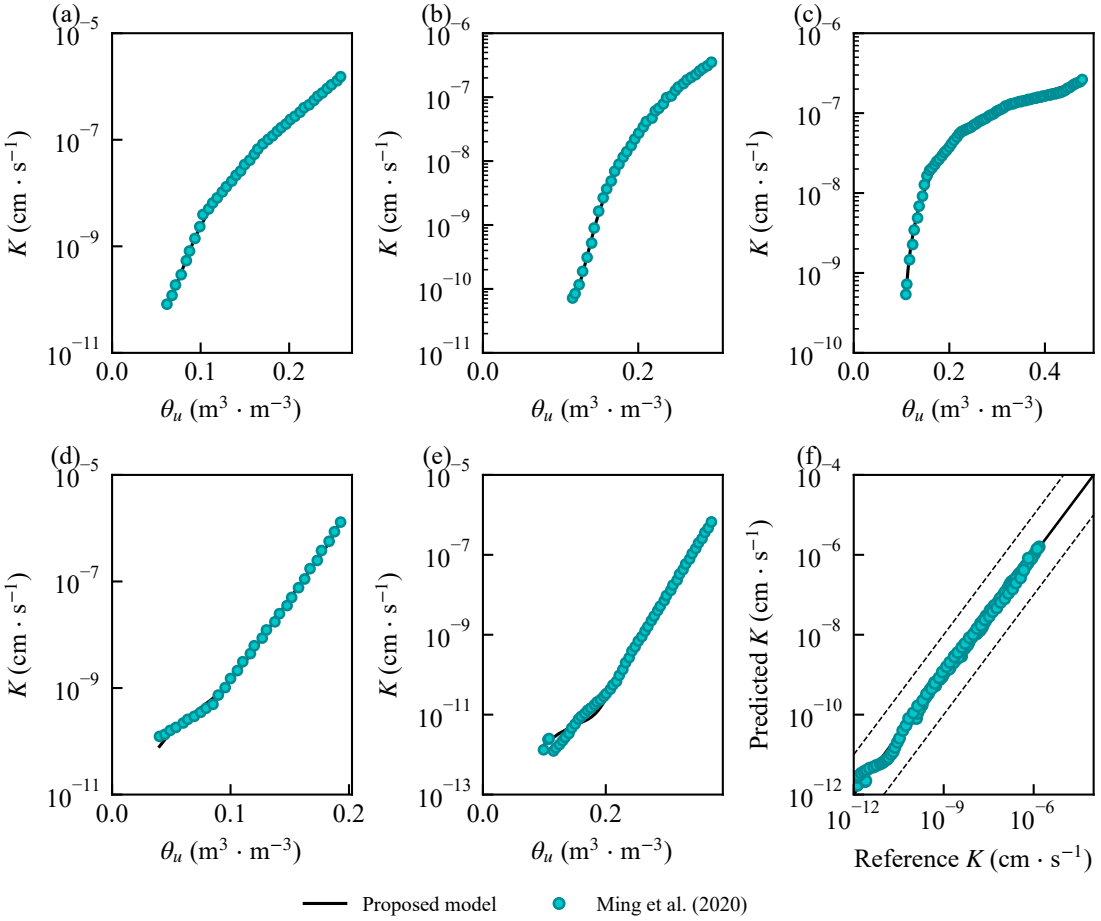

Fig. 5. Model validation against frozen soil experimental data from Ming et al. (2020). (a) Silt 1, (b) Clayey silt, (c) Silt 2, (d) Silt 3, (e) Silty clay and (f) comparison between predicted and reference hydraulic conductivity for all frozen soil samples.

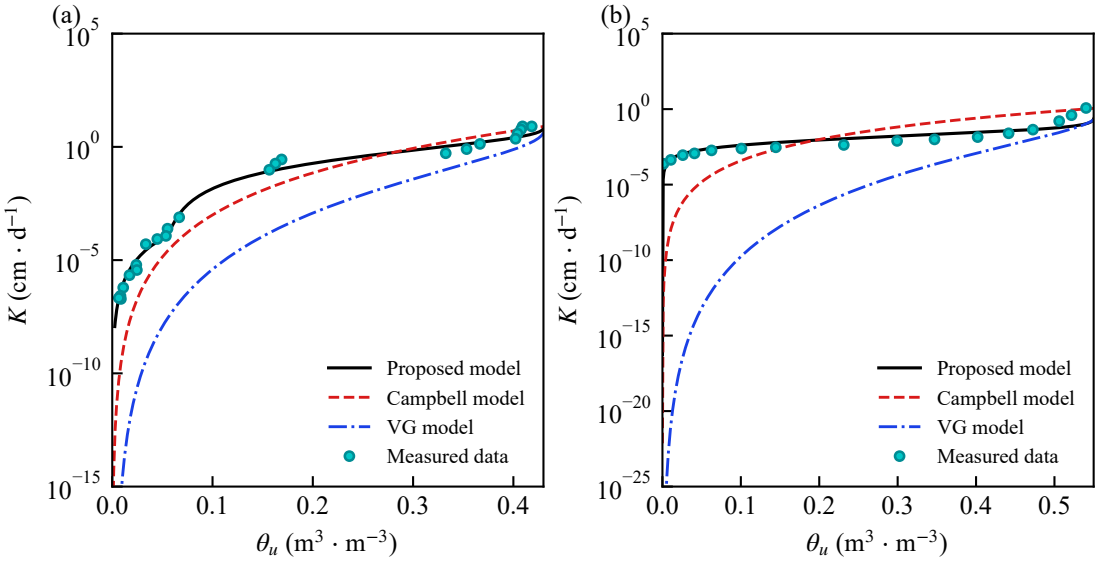

Fig. 6. Comparison of the proposed model with the Campbell model and the van Genuchten (VG) model against measured data. (a) Gilat loam and (b) Hollern clay 2.

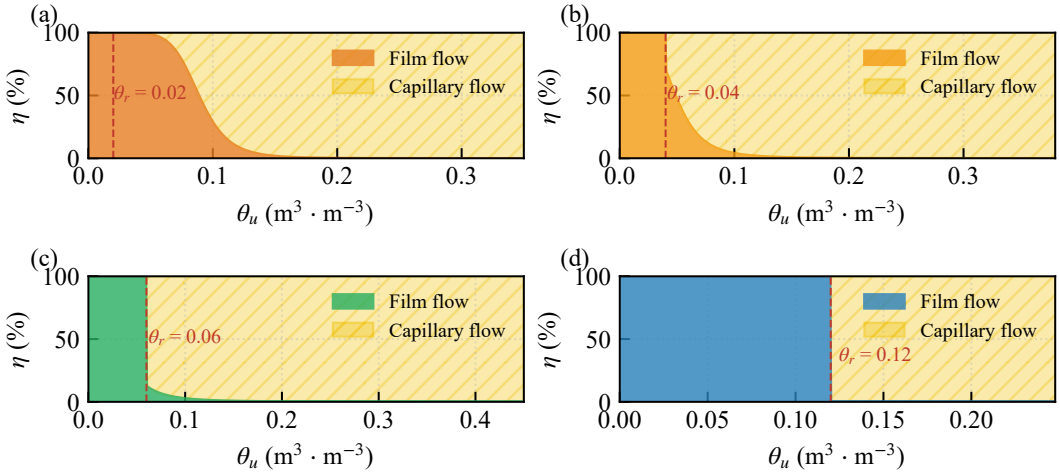

Fig. 7. Contribution ratios of capillary flow and film flow to total hydraulic conductivity as a function of volumetric water content. (a) Hupsel sand, (b) Masa loamy sand, (c) Gilat loam and (d) Hollern clay 2.

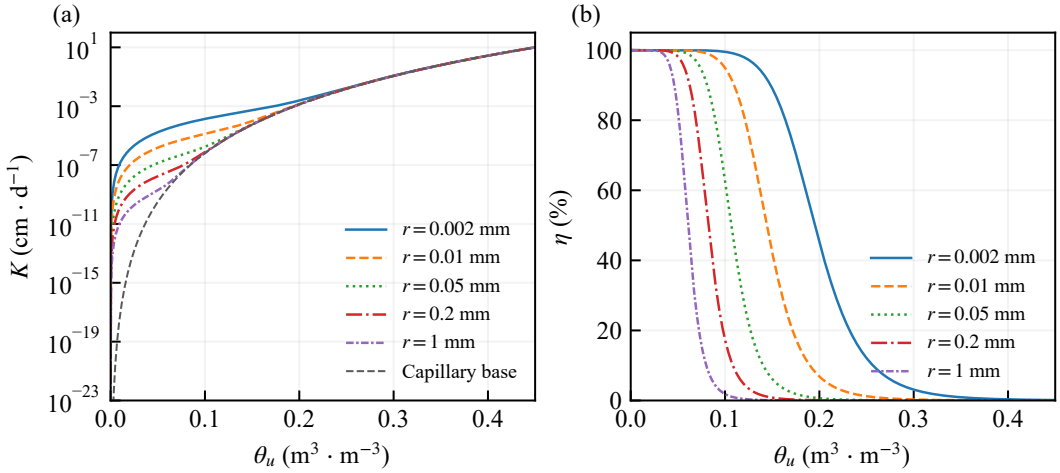

Fig. 8. Sensitivity of hydraulic conductivity and film flow contribution to pore radius. (a) Total hydraulic conductivity versus water content for varying pore radii and (b) film flow contribution ratio versus water content for varying pore radii.

film flow expression and its implications for water transport in frozen ground.

The response of total hydraulic conductivity and the film flow contribution ratio to varying equivalent particle radii (r) is shown in Fig. 8. As shown in the left panel, the influence of particle radius is minimal in the wet regime (e.g., $\theta > 0.3$), where all conductivity curves converge toward the capillary baseline. However, in the dry regime, a decrease in r significantly elevates the total hydraulic conductivity. For example, decreasing r from 1 to 0.002 mm increases total conductivity by several orders of magnitude at low water contents. Correspondingly, the right panel shows that as the particle size decreases, the S-shaped contribution curve systematically shifts to the right. This indicates that the transition from capillary-dominated to film-dominated flow occurs at much higher water contents for finer particles.

This phenomenon can be physically explained by the geometric relationship between particle size and specific surface area. The specific surface area of a soil matrix is inversely proportional to its equivalent particle radius. Finer particles, such as those in clay matrices ($r = 0.002$ mm), have a substantially larger specific surface area than coarse sand. According to the explicitly derived film flow equation, a larger specific surface area provides more surface area for water adsorption, which directly increases the baseline capacity of film conductivity. Consequently, as the capillary network desaturates or freezes, the robust film transport in fine-grained soils can overtake the rapidly decaying capillary flow much earlier. This mechanism explains why the film flow contribution reaches 100% at higher moisture levels in soils with smaller particle radii.

The effect of soil porosity on total hydraulic conductivity and flow partitioning is shown in Fig. 9. As shown in the left panel, for any given unfrozen water content (θ), a lower porosity (e.g., $\phi = 0.35$) consistently results in a higher total hydraulic conductivity compared to a higher porosity ($\phi = 0.55$). The right panel reveals that as porosity decreases, the contribution curve of film flow systematically shifts to the left. This indicates that in denser soils, the transition from capillary-dominated to film-dominated flow is delayed, occurring at a significantly lower absolute water content.

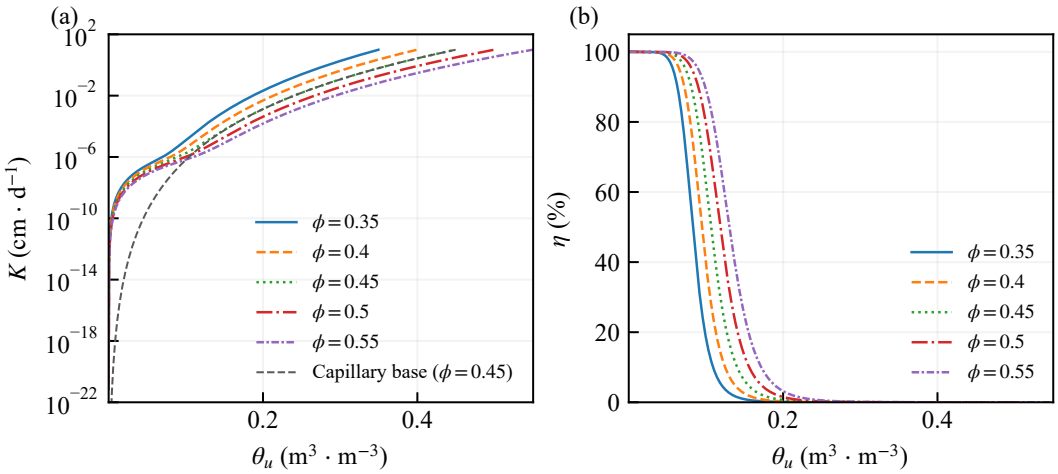

Fig. 9. Sensitivity of hydraulic conductivity and film flow contribution to porosity. (a) Total hydraulic conductivity versus water content for varying porosity and (b) film flow contribution ratio versus water content for varying porosity.

This response is governed mainly by the capillary-flow component, which relies heavily on the effective saturation ($S_e = \theta/\phi$). For a fixed volume of unfrozen water (θ), a smaller porosity (ϕ), physically representing either a more compacted soil matrix or pore space occluded by ice, forces the remaining liquid water into a more concentrated and better-connected network. Since capillary conductivity (K_c) is a high-order power function of this effective saturation, maintaining a higher S_e within these restricted microchannels preserves the hydraulic connectivity of the macroscopic capillary network longer than in a more porous matrix. Consequently, this sustained local saturation prolongs the dominance of capillary transport, shifting the onset of film flow dominance toward lower water contents in denser or more ice-filled soils.

Temperature also affects the film flow contribution through both water viscosity and film thickness. According to Eq. (13), K_f is inversely proportional to the dynamic viscosity μ and proportional to the cubic power of the film thickness f. Therefore, a decrease in temperature may reduce K_f by increasing water viscosity and thinning the unfrozen water film. Among these two effects, the change in f is expected to be more influential because of the cubic dependence in the film flow expression. This means that temperature does not act independently from the structural parameters r and ϕ. A smaller particle radius can partly sustain film flow by increasing the available surface area for adsorbed water, whereas a lower porosity or stronger ice occupation changes the effective saturation and shifts the capillary-film transition. Therefore, the temperature sensitivity of frozen soil hydraulic conductivity should be interpreted together with particle size, porosity, and the evolution of unfrozen water films.

Simulating coupled heat and water transport in cold regions requires a robust hydraulic conductivity parameterization. Currently, most large-scale land surface models and hydrological simulators (e.g., CLM, SHAW, and HYDRUS) rely on classical Mualem-van Genuchten or Campbell models to govern liquid water fluxes in freezing soils (Hansson et al., 2004; Niu and Yang, 2006). However, as demonstrated by the mechanism partitioning in this study, these classical models do not explicitly represent film flow. Consequently, under conditions of high supercooling, the macroscopic capillary network effectively ruptures, forcing the predicted hydraulic conductivity to abruptly drop to zero (Painter et al., 2013; Walvoord and Kurylyk, 2016). This nonphysical cutoff can cause non-convergence in coupled heat and water calculations and underestimate persistent winter moisture migration (Dall'Amico et al., 2011).

The continuous dual-mechanism model proposed in this study provides a physically based alternative for addressing these macroscale modeling limitations, which is also consistent with recent efforts to link pore scale transport mechanisms with macroscale flow parameterization in complex porous media (Hussain et al., 2023). By incorporating the derived film flow equation ($K_f \propto \theta^3$), the model provides a hydrodynamic baseline that maintains nonzero liquid transport in deeply frozen soils. From a numerical perspective, the smooth, self-regulating mathematical transition avoids the artificial dry-end cutoff and may improve the stability of Richards' equation solvers under freezing conditions (Zheng et al., 2021). From a physical perspective, representing this persistent microscale liquid flux is important for calculating the advective heat transport and the latent heat of fusion, which are often the dominant terms in the soil energy balance during winter (Zhang et al., 2016; Vereecken et al., 2019).

Furthermore, representing these microstructural controls in larger scale models may improve predictions of cryospheric responses. In arid permafrost regions, film driven moisture migration toward a freezing front can contribute to frost heave and subsequent thaw settlement (Vitel et al., 2016). By providing a full-range permeability function that accurately partitions capillary and film flow based on intrinsic soil properties (e.g., porosity and specific surface area), large-scale models may better delineate frost-susceptible zones and predict the dynamic evolution of winter baseflow under a warming climate (Lamontagne-Hallé et al., 2018).

The present model is mainly intended for frozen or partially frozen soils where liquid unfrozen water still forms connected or partially connected pathways along pore spaces and particle

surfaces. Several limitations should be noted. First, vapor flow is not explicitly included in the current formulation. Under very dry conditions or strong temperature gradients, vapor migration may contribute to total water transfer and should be coupled with the liquid flow formulation in future work. Second, the model assumes that the adsorbed film can provide an effective connected pathway represented by A_f. When film water becomes highly discontinuous, the actual film flow may be lower than the prediction of the continuous film approximation. Third, under extremely high ice content, pore ice may strongly isolate liquid domains and reduce the validity of the capillary-film transition assumed in the model. Therefore, the proposed formulation is most applicable to frozen or partially frozen soils in which unfrozen water films remain hydraulically effective, while additional constraints are needed for conditions dominated by vapor transport, severe film disconnection, or nearly complete pore ice blockage.

5. Conclusions

This study developed a continuous hydraulic conductivity model for frozen soils by incorporating a lubrication based film flow expression into an existing capillary-film framework. The main contribution is the derivation of film flow conductivity from thin film hydrodynamics and Newtonian viscous flow, rather than a redefinition of the capillary-film concept. This formulation links film conductivity to film thickness, water viscosity, effective flow area, and pressure gradient, thereby providing a physical basis for the nonzero hydraulic conductivity maintained at low unfrozen water contents.

Validation against 16 unfrozen soil datasets showed that the proposed model captured hydraulic conductivity over a wide texture range, from sand and loamy sand to clay, with R^2 values of 0.76 to 0.88. Additional validation using frozen soil data from Ming et al. (2020) showed that the model reproduced measured hydraulic conductivity over approximately 10^{-12} to 10^{-6} cm/s without imposing an artificial cutoff. These results indicate that the derived film flow term improves the continuity of hydraulic conductivity prediction under both low water content and freezing conditions.

The sensitivity analysis further showed that particle radius, porosity, and temperature jointly control the transition between capillary dominated and film dominated transport. A smaller particle radius increases the surface area available for adsorbed films, whereas porosity and ice occupation modify effective saturation and the capillary-film transition. Temperature affects the film flow contribution mainly through water viscosity and unfrozen film thickness, with the latter being especially important because of the cubic dependence of K_f on f.

The proposed model is most applicable to frozen or partially frozen soils where unfrozen water films remain hydraulically effective. Future work should further test the model under conditions of high ice content, strong temperature gradients, vapor transport, and possible film disconnection. Direct pore scale measurements of film connectivity and unfrozen water pathways would also help constrain the effective area factor and improve the physical interpretation of the model parameters.

Acknowledgements

This work was supported by the National Natural Science Foundation of China (No. 42472320).

Conflicts of interest

The authors declare no competing interest.

References

Azmatch, T. F., Sego, D. C., Arenson, L. U., et al. Using soil freezing characteristic curve to estimate the hydraulic conductivity function of partially frozen soils. Cold Regions Science and Technology, 2012, 83-84: 103-109.

Becher, H. H. A method for measuring unsaturated hydraulic conductivity. Journal of Plant Nutrition and Soil Science, 1971, 128(1): 1-12. (in German)

Campbell, G. S. A simple method for determining unsaturated conductivity from moisture retention data. Soil Science, 1974, 117(6): 311-314.

Chen, H., Gao, X., Wang, Q. Research progress and prospect of frozen soil engineering disasters. Cold Regions Science and Technology, 2023, 212: 103901.

Chen, L., Ming, F., Zhang, X., et al. Comparison of the hydraulic conductivity between saturated frozen and unsaturated unfrozen soils. International Journal of Heat and Mass Transfer, 2021, 165: 120718.

Dall'Amico, M., Endrizzi, S., Gruber, S., et al. A robust and energy-conserving model of freezing variably-saturated soil. The Cryosphere, 2011, 5: 469-484.

Dash, J. G., Rempel, A. W., Wettlaufer, J. S. The physics of premelted ice and its geophysical consequences. Reviews of Modern Physics, 2006, 78(3): 695-741.

Fujimaki, H., Inoue, M. A transient multistep outflow method to determine unsaturated hydraulic properties of a soil column. Vadose Zone Journal, 2003, 2(2): 154-163.

Golparvar, A., Zhou, Y., Wu, K., et al. A comprehensive review of pore scale modeling methodologies for multiphase flow in porous media. Advances in Geo-Energy Research, 2018, 2(4): 418-440.

Hansen-Goos, H., Wettlaufer, J. S. Theory of ice premelting in porous media. Physical Review E, 2010, 81(3): 031604.

Hansson, K., Šimůnek, J., Mizoguchi, M., et al. Water flow and heat transport in frozen soil: Numerical solution and freeze-thaw applications. Vadose Zone Journal, 2004, 3(2): 693-704.

Hussain, S. T., Regenauer-Lieb, K., Zhuravljov, A., et al. Asymptotic hydrodynamic homogenization and thermodynamic bounds for upscaling multiphase flow in porous media. Advances in Geo-Energy Research, 2023, 9(1): 38-53.

Ireson, A. M., van der Kamp, G., Ferguson, G., et al. Hydrogeological processes in seasonally frozen northern latitudes: Understanding, gaps and challenges. Hydrogeology Journal, 2013, 21(1): 53-66.

Jin, T., Cai, X., Chen, Y., et al. A fractal-based model for soil water characteristic curve over entire range of water content. Capillarity, 2019, 2(4): 66-75.

Kurylyk, B. L., MacQuarrie, K. T. B., McKenzie, J. M. Climate change impacts on groundwater and soil temperatures in cold and temperate regions: Implications, mathematical theory, and emerging simulation tools. Earth-Science Reviews, 2014, 138: 313-334.

Lamontagne-Hallé, P., McKenzie, J. M., Kurylyk, B. L., et al. Changing permafrost conditions influence terrestrial water storage and river discharge across the northern hemisphere. The Cryosphere, 2018, 12(11): 3501-3521.

Lamontagne-Hallé, P., McKenzie, J. M., Kurylyk, B. L., et al. Guidelines for cold-regions groundwater numerical modeling. WIREs Water, 2020, 7(6): e1467.

Lan, T., Hu, R., Zhao, B. Impact of pore-scale corner and film flows on macroscopic transport in porous media. Capillarity, 2025, 16(1): 1-4.

Lebeau, M., Konrad, J. M. A new capillary and thin film flow model for predicting the hydraulic conductivity of unsaturated porous media. Water Resources Research, 2010, 46(12): W12554.

Li, X. K., Li, X., Chen, X. S., et al. Modeling hydraulic conductivity function of frozen soil. Journal of Hydrology, 2024, 634: 131049.

Mehta, B. K., Shani, U., Guymon, G. L. Comparison of unsaturated hydraulic conductivity functions. Agricultural Water Management, 1994, 25(2): 203-213.

Ming, F., Chen, L., Li, D., et al. Estimation of hydraulic conductivity of saturated frozen soil from the soil freezing characteristic curve. Science of the Total Environment, 2020, 698: 134132.

Ming, F., Pei, W. S., Zhang, M. Y., et al. A hydraulic conductivity model of frozen soils with the consideration of water films. European Journal of Soil Science, 2022, 73(1): e13210.

Nemes, A., Schaap, M. G., Leij, F. J., et al. Description of the unsaturated soil hydraulic database UNSODA 2.0. Journal of Hydrology, 2001, 251(3-4): 151-162.

Niu, G. Y., Yang, Z. L. Effects of frozen soil on snowmelt runoff and soil water storage at a continental scale. Journal of Hydrology, 2006, 327(3-4): 448-467.

Pachepsky, Y. A., Shcherbakov, R. A., Varallyay, G. Prediction of the soil water retention curve from the soil particle size distribution and bulk density data. Agrochemistry and Soil Science, 1984, 33: 323-347.

Painter, S. L., Moulton, J. D., Wilson, C. J. Modeling challenges for predicting hydrologic response to degrading permafrost. Hydrogeology Journal, 2013, 21(1): 221-224.

Rempel, A. W., Wettlaufer, J. S., Worster, M. G. Premelting dynamics in porous media. Journal of Fluid Mechanics, 2004, 498: 227-244.

Saruya, T., Rempel, A. W., Kurita, K. Hydrodynamic transitions with changing particle size that control ice lens growth. The Journal of Physical Chemistry B, 2014, 118(47): 13420-13426.

Taber, S. The mechanics of frost heaving. The Journal of Geology, 1930, 38(4): 303-317.

Tang, R., Zhou, G., Jiao, W., et al. Theoretical model of hydraulic conductivity for frozen saline/non-saline soil based on freezing characteristic curve. Cold Regions Science and Technology, 2019, 165: 102794.

Tokunaga, T. K. Hydraulic properties of adsorbed water films in unsaturated porous media. Water Resources Research, 2009, 45(6): W06415.

van Genuchten, M. T. A closed-form equation for predicting the hydraulic conductivity of unsaturated soils. Soil Science Society of America Journal, 1980, 44(5): 892-898.

Vereecken, H., Weihermüller, L., Assouline, S., et al. Infiltration from the pedon to global grid scales: An overview and outlook for terrestrial system modeling. Vadose Zone Journal, 2019, 18(1): 180191.

Vitel, M., Maugis, P., Gouttevin, I., et al. Modeling heat and water transfer of frozen soils: Comparison of two simulation approaches of the liquid water content. Geoscientific Model Development, 2016, 9(5): 1867-1874.

Walvoord, M. A., Kurylyk, B. L. Hydrologic impacts of thawing permafrost: A review. Vadose Zone Journal, 2016, 15(6): 1-20.

Wan, J., Tokunaga, T. K. Film straining of colloids in unsaturated porous media: Conceptual model and experimental testing. Environmental Science & Technology, 1997, 31(8): 2413-2420.

Wang, H., Vanapalli, S. K. Model for predicting the hydraulic conductivity of frozen soils using the soil freezing characteristic curve. Water Resources Research, 2025, 61: e2024WR039453.

Wang, Y., Ma, J., Guan, H. A mathematically continuous model for describing the hydraulic properties of unsaturated porous media over the entire range of matric suctions. Journal of Hydrology, 2016, 541: 873-888.

Watanabe, K., Flury, M. Capillary bundle model of hydraulic conductivity for frozen soil. Water Resources Research, 2008, 44(12): W12402.

Wettlaufer, J. S. Ice surfaces: Macroscopic properties and thermodynamic influences. Physical Review Letters, 1999, 82(12): 2516-2519.

Zhang, X., Li, D., Chen, L., et al. A new integral model for predicting the hydraulic conductivity of saturated frozen soil. Journal of Hydrology, 2021, 603: 126838.

Zhang, Y., Chen, W., Riseborough, D. W. Unfrozen water contents of different soils and their implications for geoengineering in cold regions. Cold Regions Science and Technology, 2016, 123: 114-124.

Zhao, J., Liu, Y., Qin, F., et al. Pore-scale fluid flow simulation coupling lattice Boltzmann method and pore network model. Capillarity, 2023, 7(3): 41-46.

Zheng, F., Zhang, L., Ma, J., et al. Improving the numerical stability of water flow simulations in frozen soils. Journal of Hydrology, 2021, 598: 126260.

Zhou, Y., Guan, W., Zhao, C., et al. Spontaneous imbibition behavior in porous media with various hydraulic fracture propagations: A pore-scale perspective. Advances in Geo-Energy Research, 2023, 9(3): 185-197.